Olabode, Olaitan; Kosunen, Marko; Unnikrishnan, Vishnu; Palomäki, Tommi; Laurila, Tomi; Halonen, Kari; Ryynänen, Jussi

Time-based Sensor Interface for Dopamine Detection

Published in:
IEEE Transactions on Circuits and Systems - I: Regular Papers

DOI:
10.1109/TCSI.2020.3008363

Published: 01/10/2020

Document Version
Peer reviewed version

Please cite the original version:
Olabode, O., Kosunen, M., Unnikrishnan, V., Palomäki, T., Laurila, T., Halonen, K., & Ryynänen, J. (2020). Time-based Sensor Interface for Dopamine Detection. *IEEE Transactions on Circuits and Systems - I: Regular Papers*, *67*(10), 3284-3296. [9144288]. https://doi.org/10.1109/TCSI.2020.3008363

Time-based Sensor Interface for Dopamine Detection

Olaitan Olabode, Marko Kosunen, *Member, IEEE,* Vishnu Unnikrishnan, *Member, IEEE,* Tommi Palomäki, Tomi Laurila, Kari Halonen, *Member, IEEE,* and Jussi Ryynänen *Senior Member, IEEE*

***Abstract*—This paper describes the design of an integrated sensor interface for dopamine detection. The sensor interface circuit fabricated in 65 nm CMOS technology utilizes a time-based analog-to-digital conversion circuit built around a ring oscillator. The circuit supports a wide input current range of ± 1.2 μA and sampling rate of 1 - 20 kHz, enabling sub-second detection of neurochemicals within the supported current range. Measured results with physiologically relevant dopamine concentration of 500 nM demonstrate the ability of the sensor interface circuit to detect oxidation and reduction current peaks, which provides information about the release times and redox potentials of the neurochemical. This chemical information is essential in neurostimulation treatment of neurological and neurodegenerative diseases.**

***Keywords*—Neurosignal acquisition, Neurochemical sensing, Dopamine detection, Oscillator-based ADC, Biosensors, DLC.**

I. Introduction

RECENT years have witnessed an increasing interest in the detection and monitoring of neurochemicals in the brain in order to understand their relation to neurological and psychological disorders such as schizophrenia, Huntington's disease, Alzheihmer's, epilepsy, Tourette's syndrome, depression, addictions, and Parkinson's disease [1], [2]. Dopamine as a neurochemical is involved in cognitive, motor, sense of reward, and behavioral functions of the brain [1]. Thus, the detection of the release times and concentration levels of neurochemicals in the brain is highly valued in the fields of neuroscience and medical diagnostics, as it enables an improved or alternative treatment of patients suffering from psychological, behavioral, and neurodegenerative diseases.

Potentiostats are typically used to monitor neurochemicals such as dopamine, histamine and serotonin [3]. In addition, potentiostats operate based on electrochemical transduction principle. Electrochemical transduction is the process of applying a voltage (V_{cell}) across an electrochemical cell and measuring the induced reduction-oxidation (redox) current within the cell (I_{cell}) as depicted in Fig. 1. However, potentiostats are usually designed with a fixed input current range which limits the neurochemicals that can be detected by the potentiostat or sensor interface circuit. It is therefore desired to have an integrated sensor interface circuit that supports a wide input current range while maintaining high current resolution.

O. Olabode, M. Kosunen, V. Unnikrishnan, K. Halonen, and J. Ryynänen are with Department of Electronics and Nanoengineering, Aalto University School of Electrical Engineering, Espoo, Finland (email: olaitan.olabode@aalto.fi; marko.kosunen@aalto.fi; vishnu.unnikrishnan@aalto.fi; kari.halonen@aalto.fi; jussi.ryynanen@aalto.fi).

T. Palomäki and T. Laurila are with Department of Electrical Engineering and Automation, Aalto University School of Electrical Engineering, Finland (email: tommi.palomaki@aalto.fi; tomi.laurila@aalto.fi).

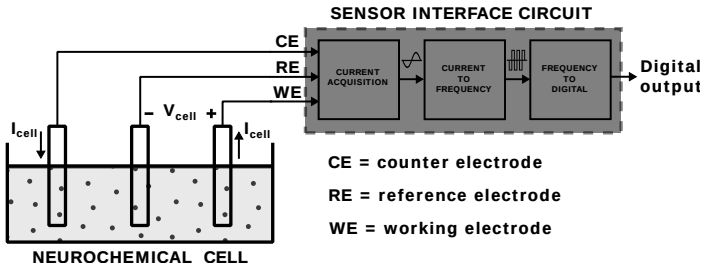

Fig. 1. System block diagram showing the neurochemical sensor electrodes which are designed to be implanted at chemical synaptic junctions in the brain and the sensor interface circuit for reading the detected cell current from the neurochemical [4].

There are several methods reported in literature for detecting neurochemicals in the brain, the most common methods being chronoamperometry (CA) and cyclic voltammetry (CV) [3], [5]. Chronoamperometry involves the application of constant potential V_{cell} across the working electrode (WE) and the reference electrode (RE), and measuring the induced current I_{cell} through the counter electrode (CE). This method is appropriate for detecting a neurochemical or biochemical when the exact potential at which the expected electrochemical reaction occurs is known such as in glucose monitoring [5], [6]. Cyclic voltammetry is used instead of chronoamperometry when the potential at which the electrochemical reaction occurs is not accurately known. This is the case for the detection of dopamine because the redox peak voltage varies for different patients and with different sensor electrode materials [7]. However, the implementation of CV is more complex because it involves applying a range of voltages V_{cell} (typically a triangular waveform) across the WE and the RE in order to obtain a full redox current I_{cell} profile of the detected neurochemical. In addition, cyclic voltammetry is especially useful for detecting both oxidation and reduction reactions of a neurochemical within the forward and reverse voltage sweep of V_{cell} respectively. Hence, the cyclic voltammetry technique is an appropriate method for dopamine detection, where both oxidation and reduction reactions are of interest for studying the release and absorption patterns of dopamine.

The main redox reactions that dopamine undergoes during cyclic voltammetry, are presented in (1) and (2), where DOQ (dopamine-ortho-quinone) is the oxidized form of dopamine (DA) [3]. This redox cycle continues for every voltage sweep of V_{cell} that is applied by the sensor interface circuit between the working electrode and the reference electrode.

$$\text{oxidation: } DA - 2e^- \Rightarrow DOQ \tag{1}$$

$$\text{reduction: } DOQ + 2e^- \Rightarrow DA \tag{2}$$

Hence, the detection of redox current peaks from the sensor interface circuit can be used to estimate the release times and stimulating potentials of the neurochemical. This information is useful for example in regulating medications and adjusting stimulation parameters during deep-brain stimulation treatment of patients suffering from neurological disorders such as Parkinson's disease, dystonia and multiple sclerosis [1], [8].

This paper presents a mixed signal sensor interface circuit for sub-second dopamine detection. The main aim of the paper is to investigate and demonstrate the possibility of detecting neurochemicals such as dopamine, using a time-based architecture and diamond-like carbon (DLC) electrodes. DLC is a novel electrode material, and only few studies have investigated its use in dopamine detection [7], [9]. Hence, the main contribution of this work is the demonstration of dopamine detection with the DLC electrodes and the proposed architecture. The proposed architecture is a combination of a transimpedance circuit topology for bi-directional current acquisition and a current-controlled oscillator based analog-to-digital converter (ADC), as an alternative sensor interface circuit for dopamine detection compared to common electrochemical potentiostats [10]. Prior dopamine detection circuits have used a combination of switched-capacitor or integrator based signal acquisition circuits and delta-sigma or single/dual-slope analog-to-digital converters [3], [11]–[14]. We believe to the best of our knowledge, that the proposed architecture is the first implementation that combines a transimpedance current acquisition circuit and current-controlled oscillator based ADC for dopamine detection application.

The proposed sensor interface circuit comprises of current acquisition, current-to-frequency and frequency-to-digital stages as shown in Fig. 1. The current acquisition circuit is connected to the counter, reference and working electrodes (CE, RE, WE) that are placed into the neurochemical cell, which models the environment in the brain. The working electrode is designed with a diamond-like carbon material which provides good sensitivity and bio-compatibility for neurochemical sensing applications [7]. The sensor interface circuit utilizes a transimpedance topology in the current acquisition stage to control the required cell voltage range from -0.7 V to 0.8 V and to support detection of a wide input current range of ± 1.2 μA. The acquired current is converted to frequency with a current-controlled oscillator (CCO). The pulses from the CCO are monitored and used to generate digital codes in the frequency-to-digital stage. The CCO-based sensor interface achieves an ENOB of 8.5 without employing any calibration or linearization techniques. In addition, the proposed circuit allows upto 20 kHz sampling rate over the supported current range. Measured results with dopamine concentration of 500 nM show that the sensor interface circuit is able to detect redox current peaks and their corresponding oxidation and reduction potentials.

The remaining part of the paper is organized as follows. Section II describes the properties of the sensor electrodes, as well as the operation and design of the sensor interface circuit. Section III presents measured results with dopamine and the DLC electrodes. Section IV concludes the discussion.

II. Operation principle of the Neurochemical Sensor Interface

A. Neurochemical Sensor Electrodes

Considering the complexity of human physiology, with thousands of reactions occurring at the same time within few milliseconds, issues such as bio-compatibility, sensitivity, and selectivity of biosensors remain main challenges [15]. In general, sensitivity and selectivity of stimulating and sensing electrodes are important requirements in the design of biosensors. Thus, the structure and selection of electrode materials strongly affects the performance of biosensors. Bio-compatibility of materials used in biosensors is also an important criteria in the selection of electrodes used in neurochemical sensing. There are several materials used in the design of neurochemical sensor electrodes. The reference electrode (RE) is usually based on silver/silver-chloride (Ag/AgCl) due to its excellent electrical and chemical characteristics such as small and stable electrode offset voltage, low electrode-solution interface impedance and low charge-transfer resistance [16]. The auxiliary or counter electrode (CE) is often based on noble metals such as platinum (Pt) or gold (Au) due to their bio-compatibility properties [3], [17]–[19]. The selection of the working electrode (WE) material is the most crucial of the three electrodes because the electrochemical reaction occurs at the surface of the working electrode. Thus, there is growing research related to the design of working electrodes compared to reference and counter electrodes.

Common working electrode materials used in the detection of neurochemicals are mainly a combination of carbon based materials, polymers, metal-oxides, and noble metals [17]. Working electrode materials are selected based on their sensitivity and selectivity to a specific neurochemical of interest, as well as their biofouling performance. Biofouling is the process of adsorption or accumulation of residual products from redox reactions onto the surface of the electrode [7]. As a result, the accumulated residue from the redox reactions changes the electrical properties of the electrode over time which causes a voltage drift in the WE voltage [20]. Consequently, the voltage drift in the WE voltage leads to inaccuracies in the measured current peaks and corresponding oxidation-reduction potentials. Hence, minimizing the effect of biofouling plays a key role in improving electrode sensitivity and resolution. Thus, design of biofouling resistant materials remains an active area of research [21], [22].

The effect of biofouling can be reduced by using carbon-based materials which are known to provide large surface area whilst having good and stable surface chemistry (i.e. charge-transfer characteristics) [17]. In addition, carbon-based materials also provide high sensitivity and improved bio-compatibility when compared with other materials. Thus, carbon-based materials and structures are effective for bio-chemical and neurochemical monitoring. Performance comparison between several carbon-based structures that are used in the detection of dopamine are summarized in Table I. It can be observed from the table that the diamond-like carbon (DLC) electrode achieves state-of-the-art performance in terms of the supported linear range and detection limits [9].

Although glassy carbon based electrodes (GCE) and carbon nanotube (CNT) structures have achieved better sensitivity, the DLC electrode provides wider linear range. Further, DLC is applied as a thin film (nm range) that can be coated on almost any substrate and therefore does not change the dimensions of the device it is deposited on. DLC is also compatible with most of the micro-and nanofabrication techniques making it suitable for device integration. GCE on the other hand, is a bulky rod that cannot be used to make devices and it is easier to modify the surface chemistry of DLC compared to glassy carbon material [22]. Table I also shows that carbon fiber microelectrodes (CFM) and interdigitated carbon electrodes have achieved lower detection limits but exhibit poor sensitivity and linear range compared to the DLC electrode. Hence, the DLC material was selected as the working electrode material because of its sensitivity, selectivity and biocompatibility performance. In addition, the DLC electrode was selected based on the following properties: fast response time, support for wide potential window, chemical inertness, low background current, ease of deposition at room temperature, compatibility with modern fabrication process, resistance to biofouling and bacterial adhesion [9], [21]–[24].

The sensitivity and selectivity of the sensor electrodes to neurochemicals such as dopamine is also important in achieving good current resolution from the sensor interface circuit. The diamond-like carbon electrodes used in this work ensure stable detection of neurochemicals and exhibit low background current (I_{bg}) in electrochemical measurements due to its high fraction of sp3-bonded carbon [7], [22]. Diamond-like carbon electrodes are also known as electrodes designed with tetrahedral amorphous carbon (ta-C) films. The sensitivity performance of the DLC electrode varies with the film thickness as observed in Table I and discussed in [9], [22]. The linear range and sensitivity values of the DLC electrodes that are presented in Table I are measured values that are defined from plotting the measured peak currents against different concentrations. Fig. 2 shows the plot for 7 nm DLC electrode and the slope of the resulting curve represents the electrode sensitivity. The limit of detection (LOD) on the other hand, is calculated as (3.3×SD)/S, where SD is the standard deviation of the measured current in blank solution (without dopamine) and S is the electrode sensitivity [9]. This implies that, the measured current from the electrode needs to be 3.3 times over the noise level for the corresponding concentration to be counted towards the LOD value. Thus, it can be observed from Table I that LOD values of 31 nM and 39 nM from 50 nm and 15 nm electrodes respectively, are higher than the lower limit of the measured linear range (10 nM) because the measured current for 10 nM of dopamine is lower than 3.3×SD. Further details about the sensitivity, selectivity and biocompatibility performance of the DLC electrodes is presented in [7], [9], [22], [23].

Likewise, the neurochemical cell impedance also contributes to the performance of the current acquisition stage. The equivalent circuit and lumped impedance model of the neurochemical cell is presented in Fig. 3, which shows the interface between the neurochemical solution and the sensor electrodes. The reference electrode is usually designed to be inert to the reactions

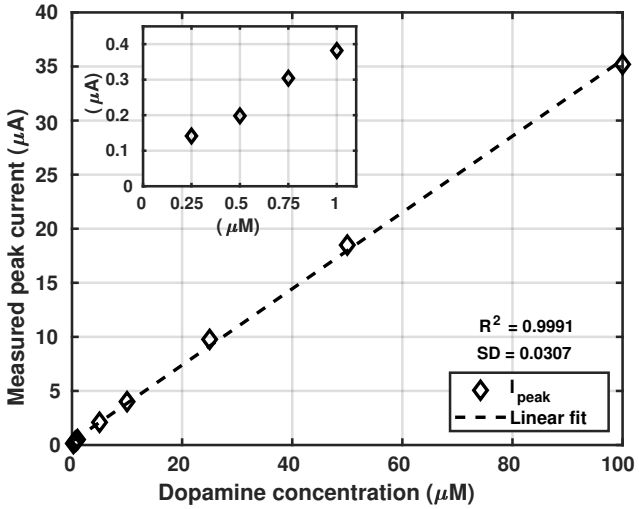

Fig. 2. Measured peak currents for different dopamine concentrations using 7 nm DLC electrode and Gamry potentiostat.

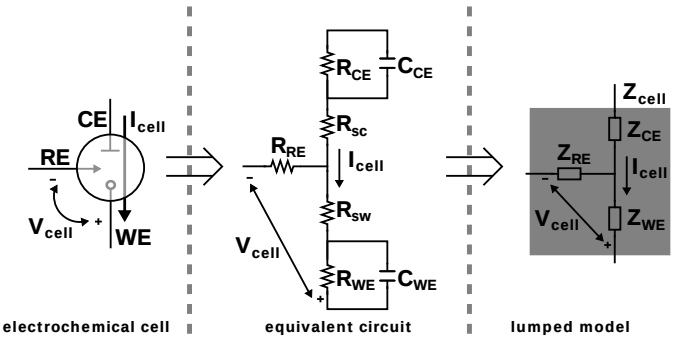

Fig. 3. Lumped impedance model of the neurochemical cell [36].

occurring within the cell and hence, its contribution to the cell impedance is negligible. The contribution of the solution resistances R_{sc} and R_{sw} to the impedance of the counter electrode (Z_{CE}) and working electrode (Z_{WE}) respectively, are also known to be negligible [35]. Thus, the impedance of the working electrode (Z_{WE}) dominates the overall impedance of the cell (Z_{cell}) since the redox reactions occur at the working electrode.

B. A/D Conversion

In recent years, there has been a gradual transition from amplitude-based processing of analog signals to time-based processing in order to leverage on the increasing speed of semiconductor processes. Hence, the CCO-based structure is selected for the proposed sensor interface because it provides ease of integration for the bi-directional current that is acquired from the cell, which leads to less complicated circuitry that is area efficient and technology-scaling friendly. The current controlled oscillator based architecture is also attractive for this application because it exhibits $\Delta\Sigma$ first-order noise shaping [37]. Thus, VCO-based quantizers are sometimes described as delta-sigma implementation in frequency domain [37].

TABLE I. COMMON WORKING ELECTRODE MATERIALS USED IN DOPAMINE DETECTION

Material and Structures	Detection limit (μM)	Sensitivity (nA/μM)	Linear range (μM)	Detection method
Diamond-like carbon (DLC) electrodes [7], [9]				
50 nm DLC film thickness	0.031	520	$0.01 - 100$	CV
15 nm DLC film thickness	0.039	280	$0.01 - 100$	CV
7 nm DLC film thickness	0.287	353	$0.25 - 100$	CV
Nafion/MWCNT [***][25], [26]	0.07	16.26 ± 1.41	$2 - 20$	DPV [**]
Poly-glutamic acid/SWCNT [***][27]	0.38	250 [*]	$3.3 - 26.6$	DPV, CV
Poly-acrylic acid/MWCNT/GCE [***][28]	0.02	4×10^3 [*]	$0.04 - 3$	DPV, CV
Methylene blue/MWCNT [29]	0.2	5.6×10^3	$0.4 - 10$	CV
Graphene modified electrode [30]	2.64	80 [*]	$4 - 100$	DPV
Nitrogen-doped graphene [31]	0.25	30	$0.5 - 170$	DPV, CV
Graphene sheets/imprinted polymers [32]	0.1	12.5	$0.1 - 830$	CV, CA, LSV [**]
Chitosan-graphene modified electrode [33]	1	20 [*]	$1 - 24$	CV
Carboxylated carbonaceous spheres (CCS)-GCE [17]	0.03	450 [*]	$0.1 - 40$	DPV
Carbon-fiber microelectrode (CFM) [3]	0.0167	10.2	$0.125 - 1$	FSCV
Interdigitated carbon electrodes [18], [34]	10^{-4}	0.57	$2 - 30$	CV

[*] estimated: actual value not explicitly defined in the source
[**] DPV: Differential pulse voltammetry, LSV: Linear sweep voltammetry
[***] MWCNT: Multi-walled carbon nanotubes, SWCNT: Single-walled carbon nanotubes, GCE: Glassy carbon electrodes

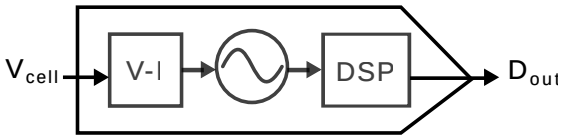

Fig. 4. Concept of the oscillator-based analog-to-digital conversion.

The principle of the oscillator-based analog-to-digital (A/D) conversion that is utilized in the sensor interface circuit is shown in Fig. 4, where the input voltage to the system controls the voltage over the cell (V_{cell}), which is transformed to current (I_{cell}) by the impedance of the electrochemical cell. The cell current (I_{cell}) is subsequently translated into time domain with the oscillator, and the time information from the oscillator is discretized by the digital signal processing (DSP) unit. Furthermore, flicker noise from the voltage-to-current converter (V-I) and oscillator stages limits the noise floor of the system at low-frequencies. In addition, presence of offsets in the V_{cell} may result in inaccuracies in the V_{cell}-I_{cell} conversion and the detected redox peak potentials. Hence, the opamps that control the V_{cell} have been designed with high gain in order to minimize offsets in the control voltage V_{cell}. The detailed structure of the time-based ADC design and noise averaging technique of the current-controlled oscillator (CCO) based A/D structure is presented in Fig. 5.

The induced current (I_{cell}) from the neurochemical cell is processed in the current acquisition (IA) stage in order to generate the control current (I_{ctrl}) for the current-to-frequency (I-F) stage. Then, a simple RC-filter is applied to I_{ctrl} for limiting the noise bandwidth. The low-pass filtered current is conveyed to the CCO which converts the current to frequency domain with I-F conversion gain (K_{cco}) as illustrated in Fig. 5. Thus, the frequency of the oscillator (F_{cco}) is modulated as the detected cell current changes. The frequency-domain information at the output of the I-F gain stage is integrated to generate changes in phase domain $\phi_{\text{cco}}(t)$. The integrator is implemented as a gray counter which is triggered at the rising edge of the generated pulses from the CCO. Use of gray counter limits the error at the sampling instances of the following derivator stage to one LSB. This is required as the current controlled oscillator is asynchronous with the sampling clock of the following derivator stage. Thus, the use of gray-encoding increases the reliability of digital code representation of the detected dopamine concentration, making the design of the sensor interface circuit more robust. The CCO-based analog-to-digital conversion with integrate-and-differentiate structure results in a cascaded-integrator-comb (CIC) filter which has a continuous-time *sinc* frequency response, and allows for noise averaging and prevents aliasing of wide-band noise into the signal band [38], [39].

C. Circuit Level Design

1) Current Acquisition (IA): The current acquisition stage of the sensor interface circuit controls the cell voltage (V_{cell}) that is applied across the WE and RE of the neurochemical cell as illustrated in Fig. 6. The applied V_{cell} is controlled based on cyclic voltammetry sweep of the input voltage (V_{in}) in order to monitor the neurochemical cell current (I_{cell}) that is flowing between the CE and WE. Several signal acquisition architectures such as grounded-WE, grounded-CE, transimpedance, and current conveyor configurations were explored [10]. The transimpedance topology presented in Fig. 6 is well-suited to

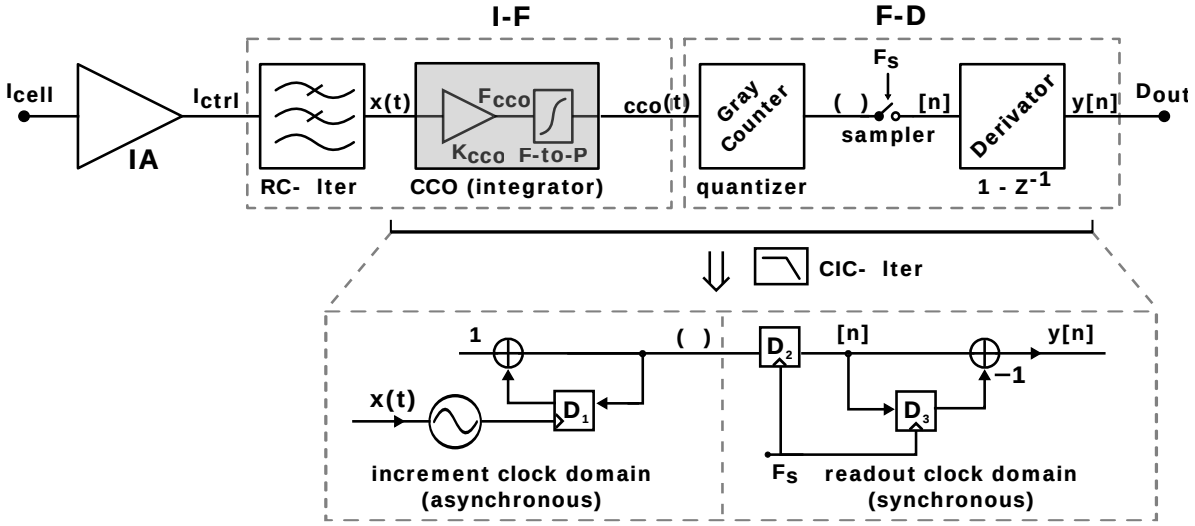

Fig. 5. System architecture of the CCO-based ADC [4].

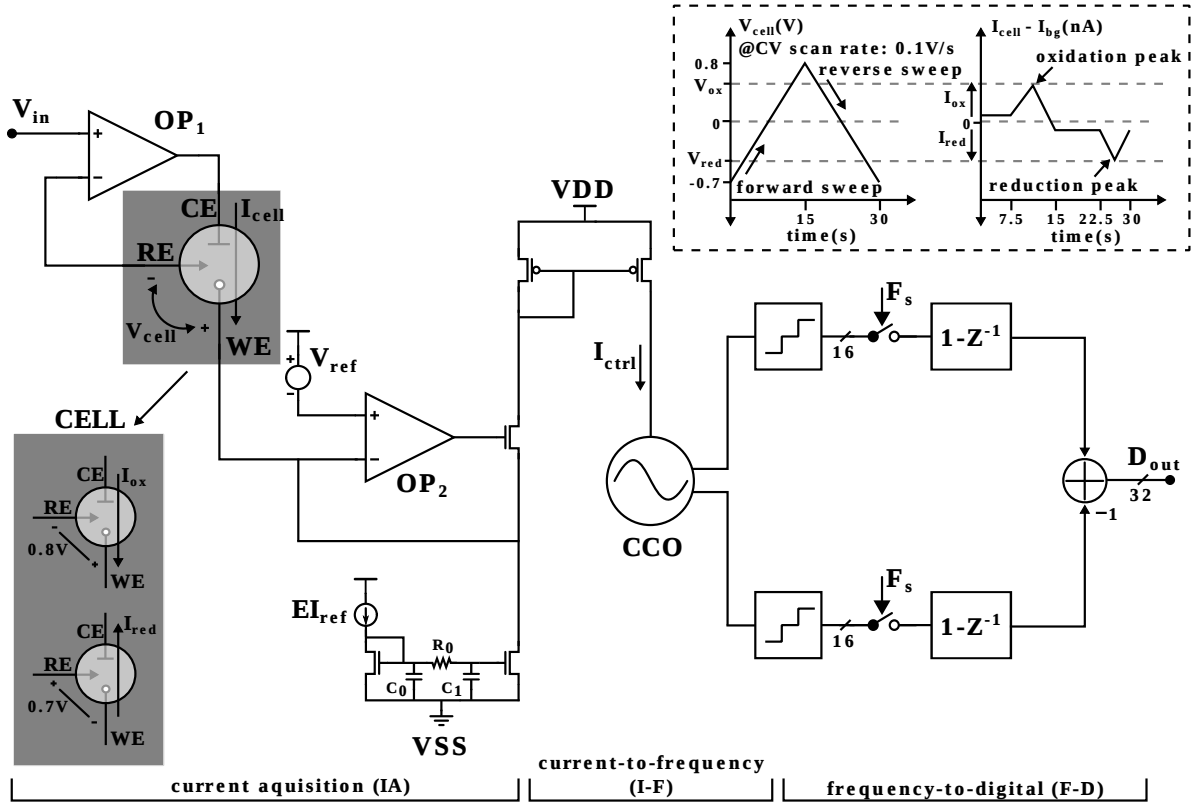

Fig. 6. Schematic of the time-based sensor interface circuit [4].

meet the design requirements of the sensor interface. This is mainly attributed to its support for the detection of bi-directional currents (I_{ox}, I_{red}) from the oxidation and reduction reactions occurring at the working electrode (WE). In addition, the topology provides a flexible way of extending the redox current range by adjusting the reference current (EI_{ref}) that is used for subtraction or addition of the I_{cell} from the sensor electrodes. The primary function of both operational amplifiers (opamp) is to provide a stable voltage over the neurochemical cell which is modelled in Fig. 3. The cell voltage is defined by ensuring that the voltage at the working electrode (V_{WE}) remains at a virtual ground defined by the input voltage of

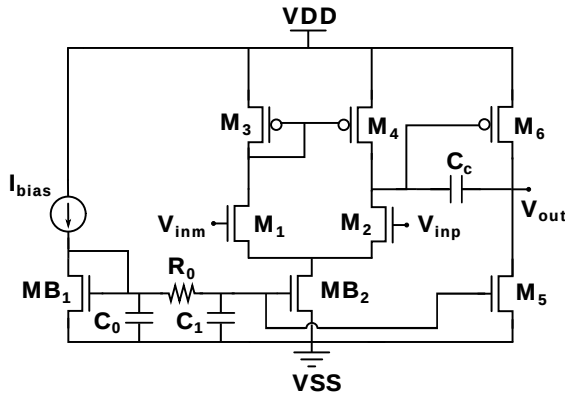

Fig. 7. Miller NMOS opamp with low-pass RC-filter [36].

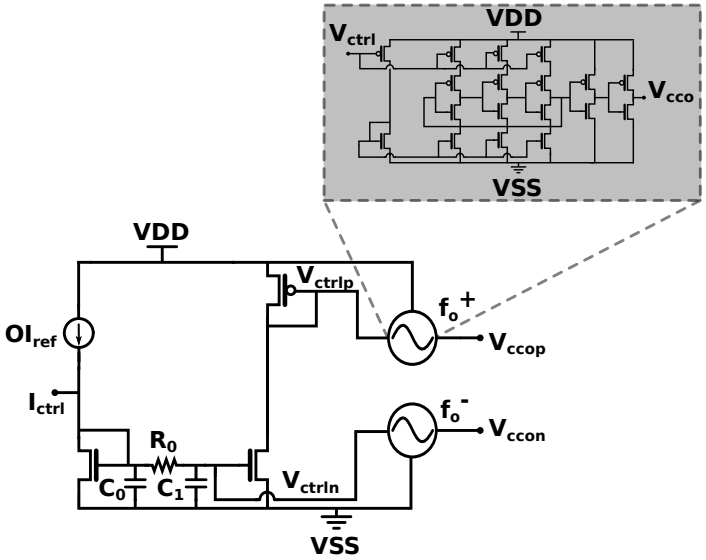

Fig. 8. Current controlled oscillator (CCO) schematic [36].

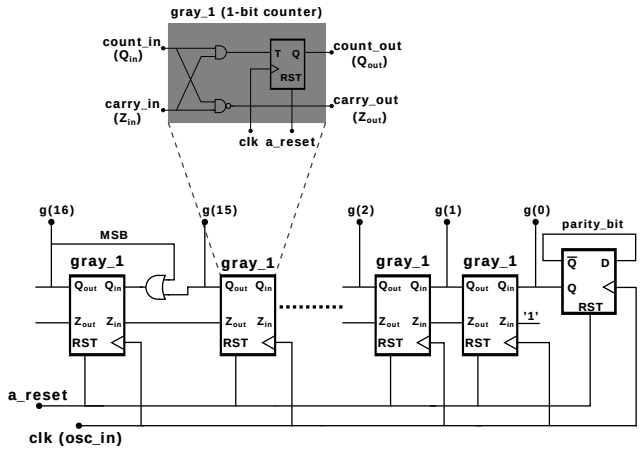

Fig. 9. 16-bit Gray code counter schematic [36].

OP_2 (V_{ref}) while the voltage at the reference electrode (V_{RE}) follows the input voltage of OP_1 (V_{in}).

The current acquistion (IA) stage is designed to provide stable V_{cell} between -0.7 V to 0.8 V potential window based on cyclic voltammetry sweep of the input voltage (V_{in}). The oxidation (I_{ox}) and reduction (I_{red}) current peaks from the neurochemical can be detected during the forward and reverse sweep of the input voltage as illustrated in Fig. 6. The potential window of 1.5 V defines the input common-mode range (ICMR) and determines the minimum supply voltage of the operational amplifiers. The operational amplifiers, OP_1 and OP_2 are designed using the 2-stage Miller-compensated opamp architecture shown in Fig. 7 because it provides good stability performance compared to the composite-cascode and folded cascode opamp architectures that were explored. Post-layout simulated performance of the opamp is presented in Table II.

Further, a simple low-pass RC-filter is implemented with R_0, C_0 and C_1 to limit high-frequency noise in the bias path of the opamp (I_{bias}). Similar RC-filter is utilized on the current acquisition and oscillator reference current paths. The bias currents (I_{bias}, EI_{ref}, OI_{ref}) and reference voltage V_{ref} are provided off-chip from the measurement printed circuit board (PCB). In addition, the opamps can operate with supply voltage range of 1.8 V to 2.5 V in order to support a wide range of V_{cell} based on the potential window required by the neurochemical and the sensor electrodes for CV measurements. Thus, a wider potential window of V_{cell} than the required 1.5 V can be achieved by setting the supply voltage of the opamps between 1.9 V and 2.5 V. High gain from the opamps reduces the effect of amplifier induced nonlinearity, which can result in unintended offset in the voltage over the electrodes V_{cell}. In addition, the opamp is designed to provide high gain of 80 dB and phase margin of 84.4^o, in order to maintain stable and accurate control of V_{cell}. The opamps OP_1 and OP_2 control V_{cell} by setting the voltage at the reference and working electrodes respectively as [4]

$$V_{\text{cell}} = V_{\text{WE}} - V_{\text{RE}} = V_{\text{ref}} - V_{\text{in}} \ . \tag{3}$$

Hence, the ratio of the applied V_{cell} to the total impedance of the cell (Z_{cell}) defines the acquired cell current as [4]:

$$I_{\text{cell}} = \frac{V_{\text{cell}}}{Z_{\text{cell}}} = \frac{V_{\text{cell}} - V_{\text{in}}}{Z_{\text{cell}}} \ . \tag{4}$$

2) Current-to-Frequency (I-F): The controllable bias current (I_{ctrl}) that flows into the oscillator decreases or increases from the defined IA reference current EI_{ref}, based on the acquired redox current I_{cell} from the neurochemical as [4]:

$$I_{\text{ctrl}} = EI_{\text{ref}} \mp I_{\text{cell}} \ . \tag{5}$$

Thus, EI_{ref} can be re-configured to support a wide range of I_{cell} within ± 1.2 μA. This flexibility in the transimpedance structure makes the circuit well-suited for neurochemical sensing applications.

The circuit implementation of the current controlled oscillator in the current-to-frequency (I-F) stage is presented in Fig. 8. The CCO is implemented with two current-starved ring oscillators operating at 1 V supply. The CCO has an internal

TABLE II. POST LAYOUT PERFORMANCE SUMMARY OF THE OPAMP USED IN THE IA BLOCK

Design parameters	Simulated results
DC open-loop gain	80 dB
Phase, Gain margin	84.4^o, 34 dB
Unity gain bandwidth (GBW)	150 kHz
Input common-mode range (ICMR)	0.2 V to 2.4 V
Output voltage swing	2.2 V
Common-mode rejection range (CMRR)	95 dB, @100 Hz 90 dB, @100 kHz
Supply voltage range	1.8 V to 2.5 V
Current consumption	2.95 μA
Power consumption (@1.8 V supply)	5.35 μW

reference current (OI_{ref}) that defines the center frequency of the oscillator. The frequency of the oscillator (F_{cco}) increases or decreases from the center frequency based on the control current I_{ctrl}. The frequency range of each ring oscillator is defined by the difference between the maximum frequency $F_{\text{cco}}(\text{max})$ and the minimum frequency $F_{\text{cco}}(\text{min})$ that corresponds to the cell current range. Thus, the dynamic range (DR) of the sensor interface circuit is determined by the frequency range of both ring oscillators and the sampling rate defined in the F-D stage [4].

$$DR \approx 20log_{10}\left(2 \cdot \left(\frac{F_{\text{cco}}(\text{max}) - F_{\text{cco}}(\text{min})}{F_s}\right)\right) \quad (6)$$

3) Frequency-to-Digital (F-D): The pulses from the oscillator outputs are quantized with two 16-bit gray code counters. The F-D stage operates with 1 V supply and the schematic of the 16-bit gray code counter is presented in Fig. 9. The accumulated counter codes are sampled with the sampling clock (F_s) and a difference operation is performed on the sampled counter codes for noise-shaping. The noise averaging operation of the F-D stage is based on the principle of cascaded integrated comb (CIC) filters as described in discrete time by (7) and Fig. 10.

$$w[n] = x[n] + w[n-1] \quad (7.a)$$
$$y[n] = w[n] - w[n-N] \quad (7.b)$$
$$y[n] = x[n] + x[n-1] + x[n-2] + ... + x[n-(N-1)] \quad (7.c)$$

CIC filter based structures are used for implementing decimation or interpolation functions in various applications related to high data rate processing [40], [41]. These applications include modulation and demodulation in wireless systems, digital-to-analog (D/A) and analog-to-digital (A/D) converters [41]. The typical structure of CIC decimation filter is presented in the (A) part of Fig. 10 and the (B) part of Fig. 10 shows the structure used in the F-D block. Both structures are equivalent in functionality but the CIC filter structure used in the F-D block

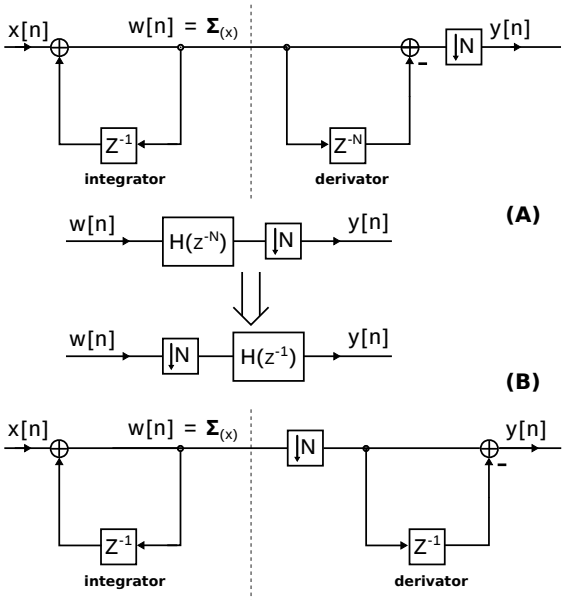

Fig. 10. Filtering principle of the frequency-to-digital stage, where (A) represents the conventional CIC decimation filter structure and (B) is the equivalent CIC filter structure that is used in the F-D stage for reducing power consumption.

is especially effective in reducing power consumption due to reduced sampling rate before derivation is performed [41].

The use of CIC filters as part of the noise averaging process is known to be effective in preventing aliasing of wide-band noise into the signal bandwidth, which alleviates the need for an anti-aliasing filter in the ADC [40], [42], [43]. However, it should be noted that a pre-filter can still be applied before the A/D conversion in order to limit the noise bandwidth. In addition, the combination of using the oscillator as an integrator together with the counter as a quantizer and differentiator eliminates the need for sample and hold stage during the A/D conversion [42]–[44]. Other advantages of using this ADC structure include reduction in the effect of DC offset and filtering of high-frequency noise [42], [44], [45]. This is a result of its inherent low-pass characteristic based on its *sinc* filter transfer function which is derived from (7) as:

$$W(z) = \frac{X(z)}{1 - z^{-1}} \quad (8.a)$$
$$Y(z) = W(z) * (1 - z^{-N}) \quad (8.b)$$
$$Y(z) = \left[\frac{X(z)}{1 - z^{-1}}\right] * (1 - z^{-N}) \quad (8.c)$$
$$\Rightarrow H(z) = \frac{Y(z)}{X(z)} = \frac{1 - z^{-N}}{1 - z^{-1}} \quad (8.d)$$

III. MEASUREMENT RESULTS

The measurement setup for the detection of dopamine with the sensor interface circuit requires preparation of the DLC electrodes and the dopamine solution. The dopamine solution used during the measurements was prepared by adding

(a) (b)

Fig. 11. Dopamine solution and sensor electrode preparation: DLC samples are attached to copper contact strips which enables connection of the electrodes to the measurement board.

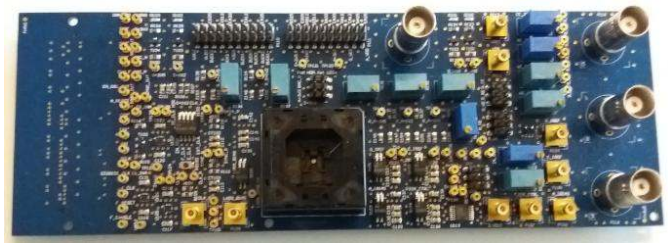

Fig. 12. Measurement printed circuit board which connects the sensor interface chip to the sensor electrodes.

Dopamine hydrochloride (Sigma-Aldrich) to a phosphate-buffered solution (PBS) with pH value of 7.4. The dopamine solution is prepared in a three-channel glass beaker as shown in Fig. 11a while Fig. 11b shows a few DLC electrode samples attached to copper strips, which enable connection of the electrodes to the printed circuit board. The measurement board shown in Fig. 12 provides three BNC connectors for connecting the chip to the sensor electrodes and an integrated circuit (IC) socket to hold the sensor interface chip housed in Quad Flat No Leads (QFN) 32-pin package. Fig. 13a shows the die micrograph of the sensor interface chip fabricated in 65 nm CMOS technology. The processing blocks of the sensor interface circuit occupy an area of 0.059 mm^2 (IA: 0.019 mm^2, I-F: 0.005 mm^2 and F-D: 0.035 mm^2).

Cyclic voltammetric measurements were performed in a three-electrode setup with a Ag/AgCl reference electrode (Radiometer Analytical), a graphite rod as a counter electrode, and the DLC working electrode. The working electrode is designed with a 7 nm DLC film thickness and an average surface roughness of 1.6 nm. Thus, the 7 nm DLC electrode sensitivity that is reported in Table I can be used as a reference to compare the measured peak current from the sensor interface. The DLC film was deposited with a filtered cathodic vacuum arc (FCVA) system on a 20 nm Ti inter-layer on top of p-type Si (100). The DLC electrode surface topography is presented in Fig. 13b as taken from an atomic force microscope (AFM).

The required input voltage range of 1.5 V is applied to the sensor interface circuit input (V_{in}) at 100 mV/s sweep rate for the CV measurements, which in turn controls the cell voltage between WE and RE and defines the redox potential window (-0.7 V to 0.8 V) for the acquisition of the cell current. The

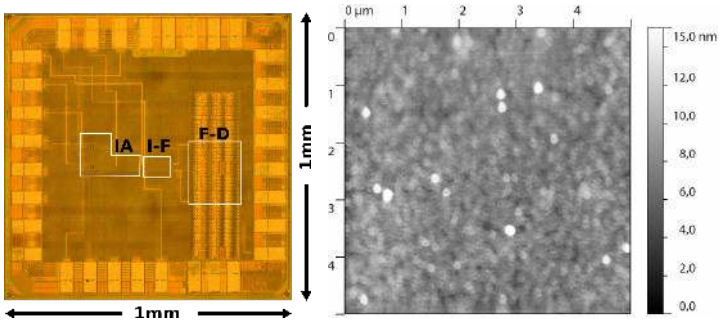

(a) (b)

Fig. 13. Die micrograph of the sensor interface chip in 65 nm CMOS technology and topography map of the DLC electrode surface.

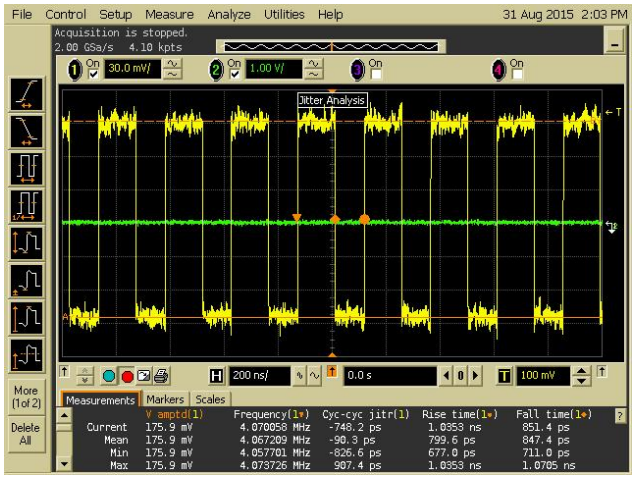

Fig. 14. Single oscillator output (F_{ccop}) waveform, where the vertical axis scale is 30 mV/div and horizontal axis scale is 200 ns/div.

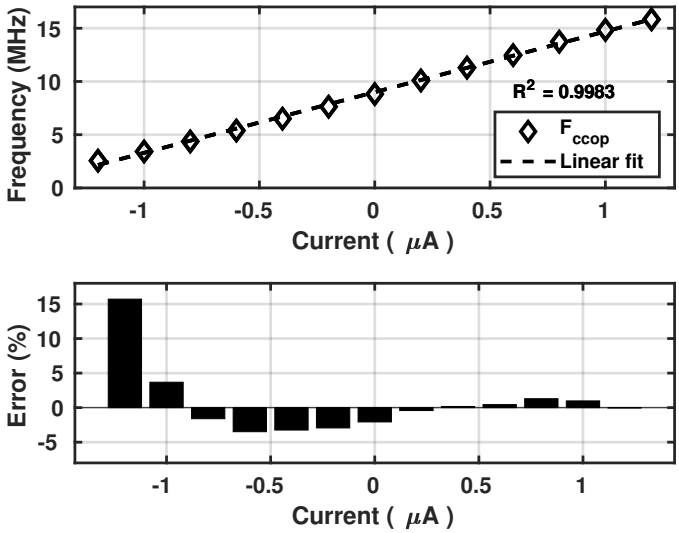

Fig. 15. I-F transfer characteristics for single oscillator output (F_{ccop}).

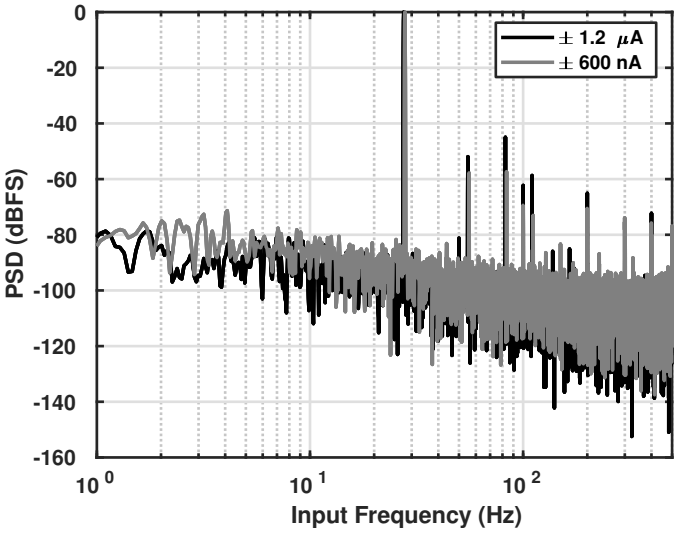

Fig. 16. Measured output spectrum at full scale input (± 1.2 μA) and at peak performance (± 600 nA), from 2^{14} digital output codes sampled at 1 kHz.

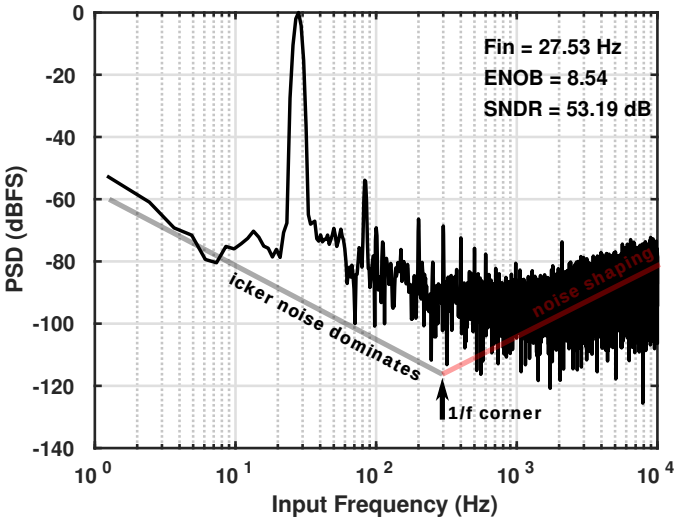

Fig. 17. Measured output spectrum of ± 600 nA input at 20 kHz sampling rate. The noise bandwidth is 500 Hz and the 1/f corner occurs at $\sim$300 Hz.

acquired cell current controls the oscillator and the raw pulses from one of the oscillator outputs F_{ccop} is shown in Fig. 14. In addition, Fig. 15 shows the current-to-frequency transfer characteristics and linearity error from the F_{ccop} oscillator output for the supported cell current range of ± 1.2 μA. The coefficient of determination (R^2) from the I-F transfer curve is 0.9983 and the linearity error from the current-to-frequency conversion increases as the input current amplitude increases. The pulses from each oscillator are processed in the frequency-to-digital block and the 16-bits digital output code from each differential path is combined as a 32-bits word and serialized out of the chip with a synchronization flag indicating the start of each 32-bits word, which corresponds to the sampling rate (F_s) of the digital output.

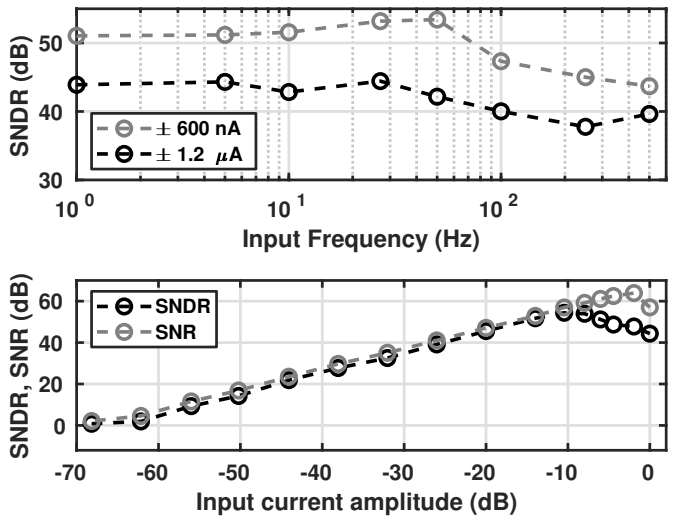

Fig. 18. ADC performance with respect to input frequency and amplitude.

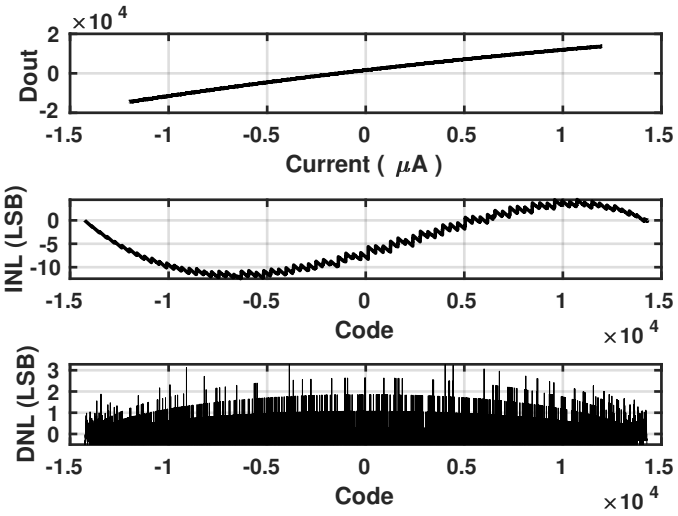

Fig. 19. Digital output codes (D_{out}) for I_{cell} range = ± 1.2 μA and static linearity performance from the digital output codes.

The measured power spectral density (PSD) of the digital output codes sampled at 1 kHz in response to single-tone sinusoidal inputs (± 1.2 μA and ± 600 nA) is shown in Fig. 16. The output spectrum of ± 600 nA input sampled at 20 kHz is presented in Fig. 17, which shows that the converter supports noise-shaping and achieves an effective number of bits (ENOB) of 8.5 at peak SNDR of 53.19 dB. The noise bandwidth for the measured output spectrum is 500 Hz. The performance of the ADC with respect to input frequency and input current amplitude is shown in Fig. 18. The dynamic performance of the converter shows that the sensor interface circuit is able to provide sub-second detection over a wide range of current input (± 1.2 μA), which enables detection of various neurochemicals other than dopamine.

Furthermore, the static linearity performance of the converter is evaluated from the measured current-to-digital transfer

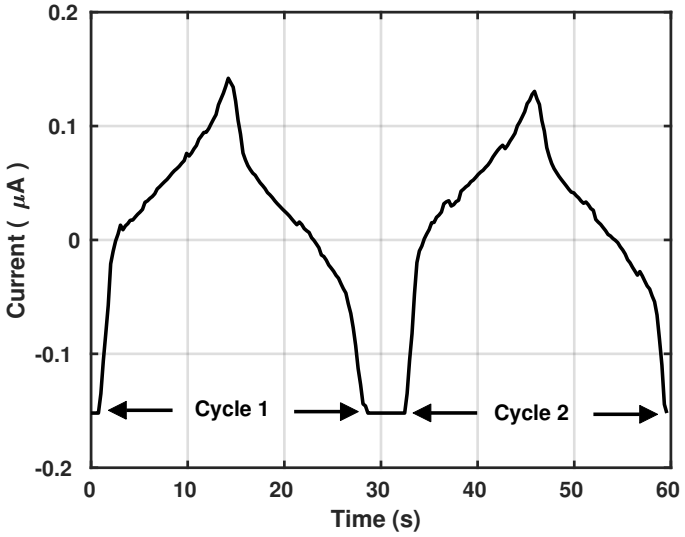

(a) I_{bg} from PBS solution

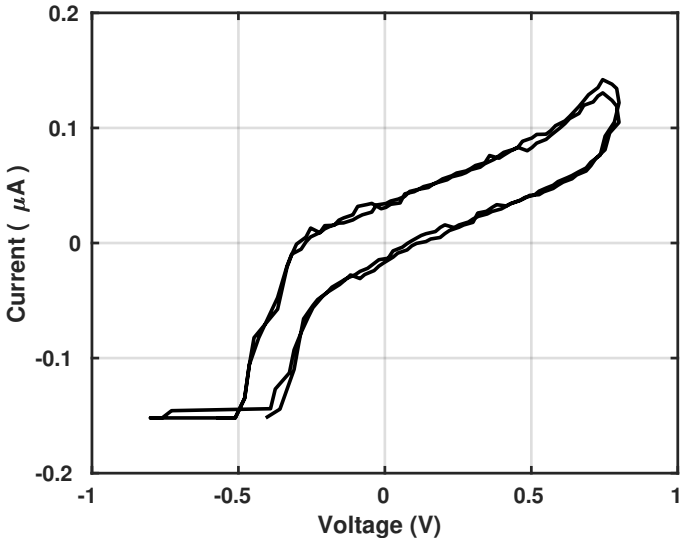

(b) Cyclic voltammetry of I_{bg}

Fig. 20. Readout of I_{cell} (i.e. $I_{\text{ctrl}} - EI_{\text{ref}}$) from phosphate-buffered solution (PBS) which represents the background current I_{bg} in Fig. 20a and the corresponding cyclic voltammetry (CV) profile in Fig. 20b.

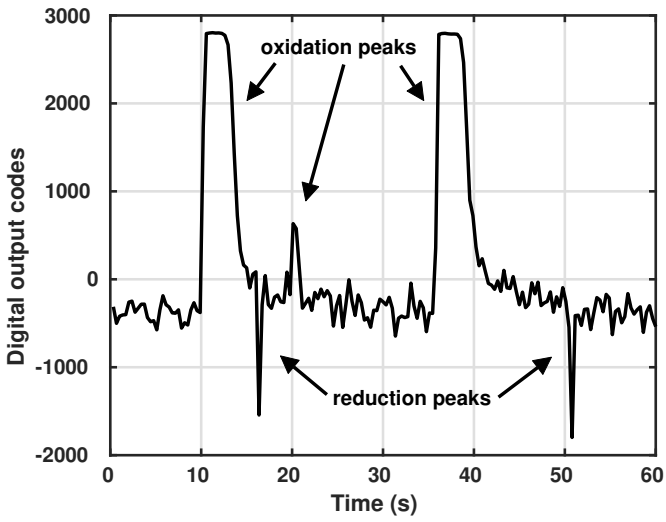

(a) D_{out} from 500 nM of dopamine

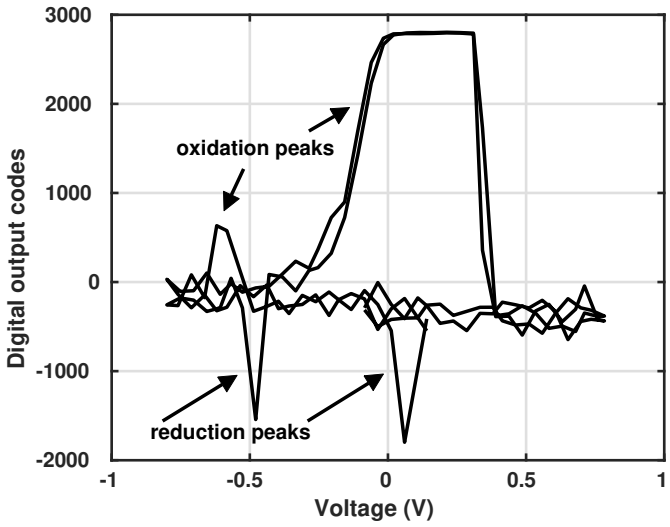

(b) CV of the detected I_{cell} codes

Fig. 21. Digital output codes from PBS and 500 nM of dopamine showing the oxidation-reduction peaks is observed in Fig. 21a and the corresponding oxidation-reduction potentials at which the redox peaks occur is observed in Fig. 21b.

curve and presented in Fig. 19. The digital output code range corresponding to the cell current range ± 1.2 μA is 28098 LSBs (88.97 dB), which is defined by the oscillation frequency range (F_{cco}) and the sampling rate (F_s) as given in equation (6). Although, the sensitivity of the current-to-digital conversion covers a wide range, the accuracy (i.e. linear range) is limited by the non-linearity of the current-to-frequency conversion which is visible from Fig. 15. Nonetheless, the accuracy of the converter improves for lower current amplitudes (± 600 nA) compared to the full scale current range.

The acquisition of the cell current from PBS solution is shown in Fig. 20a for 2 V_{cell} sweep cycles. The acquired current from PBS serves as the background current estimate (I_{bg}), which is subtracted when dopamine is added to the measurement setup. As a result, the background subtracted cell current ($I_{\text{cell}} - I_{\text{bg}}$) represents the change in current due to oxidation and reduction of dopamine. The cyclic voltammetry measurement from the PBS solution is presented in Fig. 20b and it is important to note that the observed upward progression of the CV measurement occurs due to the presence of oxygen in the neurochemical cell which depicts the environment in the brain. This demonstrates that using the DLC working electrode with the sensor interface circuit results in relatively stable detection of the background current also in the presence of oxygen due to the properties of the DLC electrode.

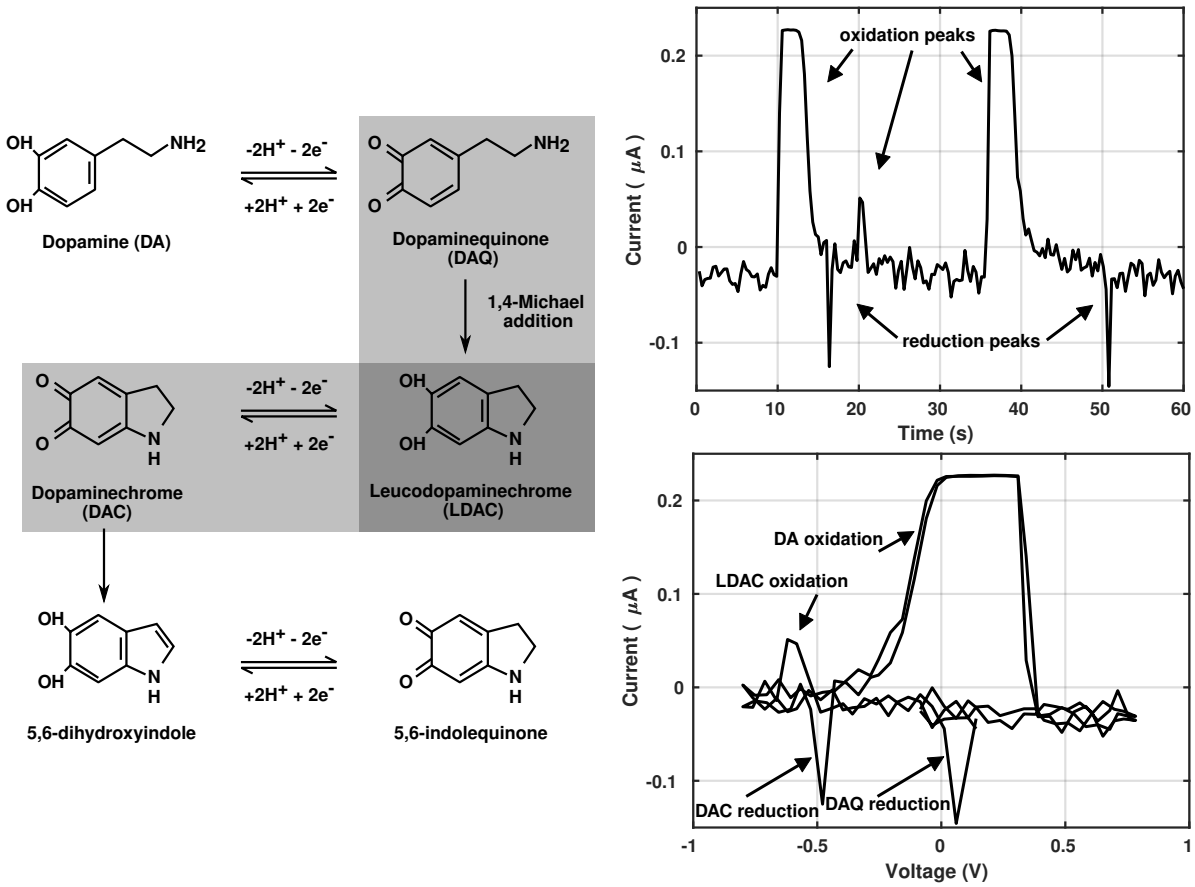

Fig. 22. Readout of I_{cell} from PBS and 500 nM dopamine solution, and the oxidation-reduction reactions that dopamine undergoes [46].

Furthermore, 500 nM of dopamine is added to the PBS solution and Fig. 21a and Fig. 21b show the digital output from the sensor interface circuit at 1 kHz sampling rate. The oxidation and reduction peaks due to the presence of dopamine are also visible. In addition, Fig. 22 shows the cell current that is obtained when 500 nM of dopamine is added to the PBS solution. The peak current of 0.226 μA from Fig. 22 is comparable to the 7 nm DLC electrode sensitivity in Fig. 2 and Table I. Fig. 22 also presents the oxidation process of dopamine which may involve additional redox reactions if the CV sweep rate is slow (typically 50 - 500 mV/s) [9], [21], [46]. These additional chemical reactions occur after the oxidation of dopamine (DA) to dopaminequinone (DAQ) because there is enough time for them to occur before DAQ is reduced back to DA on the reverse sweep. The sweep rate of the measurement setup is 100 mV/s which allows oxidation of dopamine (DA) to dopaminequinone (DAQ), and oxidation of leucodopaminechrome (LDAC) to dopaminechrome (DAC). The main redox peaks from DA and DAQ occurs around +0.1 V and the additional redox peaks related to LDAC and DAC occurs around -0.5 V as observed in Fig. 21 and Fig. 22.

Typical dopamine concentration in the brain is reported to be within 10 nM - 1 μM [7]. Hence, the sensor interface circuit is able to detect physiologically relevant concentration of dopamine. The main contributors to the dopamine concentration detection limit of the overall system is a combination of the electrode and the sensor interface sensitivity. The focus of the paper is to demonstrate the possibility of detecting dopamine with the DLC electrode material and the time-based sensor interface. These measured results show that the sensor interface is able to detect both the first and second redox reactions if they occur. As a result, the detection of the redox peaks is useful in providing a profile of the oxidation and reduction potentials prior to neurostimulation treatment.

Table III presents the summary of the measured performance of the sensor interface circuit and comparison with some prior work in similar application area for dopamine detection. It can be observed from the table that this work can operate with low supply voltage of 1.8 V and provides support for a wide range of input current ($\pm$1.2 μA) when compared to other works. In addition, the proposed structure provides an alternative to the delta-sigma and single/dual-slope implementations that are used in other works. However, the SNDR of the CCO-based sensor interface is limited by the non-linearity of the current-to-frequency conversion. Nonetheless, the converter achieves an ENOB of 8.5 without employing any calibration or linearization techniques. The converter also supports upto 20 kHz sampling rate over a wide current range. As a result,

TABLE III. PERFORMANCE COMPARISON WITH PRIOR DOPAMINE DETECTION CIRCUITS

Design parameters	This work	TBCAS 17, [11]	TBCAS 16, [12]	JSSC 14, [13]	TBCAS 13, [14]	JSSC 09, [3]
Technology (CMOS)	65 nm	65 nm	0.35 μm	0.35 μm	0.35 μm	0.5 μm
Electrode material	DLC	Graphene	CFM	CFM	Gold (Au)	CFM
Detection circuit	CCO-based ADC	Dual-slope ADC	$\Delta\Sigma$ ADC	$\Delta\Sigma$ ADC	Single-slope ADC	$\Delta\Sigma$ ADC
Input current range	$\pm$1.2 μA	$\pm$165 nA	$\pm$900 nA	$\pm$950 nA	$\pm$175 nA	$\pm$750 nA
Control voltage range	1.5 V	1.7 V	1.7 V	1.7 V	1 V	1.4 V
(CV potential window)	($-$0.7 V, 0.8 V)	($-$0.4 V, 1.3 V)	($-$0.4 V, 1.3 V)	($-$0.4 V, 1.3 V)	($-$0.1 V, 0.9 V)	($-$0.4 V, 1 V)
Sampling rate	$1-20$ kHz	$5-10$ kHz	9.77 kHz	10 kHz	0.1, 1 kHz	10 kHz
Peak SNDR	53.19 dB	62.4 dB	72.1 dB	70.7 dB	-	-
Supply voltage	1.8 V	1.8 V	2.5 V	2.5 V	3.3 V	$\pm$1.25 V
Power consumption	49 μW	3.1 μW	9.5 μW	74.5 μW	188 μW	76 μW
	18 μW (IA stage)*		(duty-cycled)**	9.3 μW (duty-cycled)**		

*power consumption of current acquisition stage, **average consumption in power-saving mode

the sensor interface circuit enables detection of a wide range of neurochemicals other than dopamine and can also be used in current sensing applications.

IV. CONCLUSION

This paper describes the design of a time-based sensor interface circuit with wide input current range for dopamine detection. The circuit is fabricated in a 65 nm CMOS process. Measured results show that the sensor interface circuit can detect redox peaks from physiologically relevant dopamine concentration of 500 nM with novel diamond-like carbon sensor electrodes. Hence, the detected oxidation and reduction current peaks from the sensor interface circuit allows monitoring of the release times of neurochemicals in the brain and suitable stimulating potentials. The achieved current range of $\pm$1.2 μA makes the sensor interface well-suited for neurochemical sensing applications.

The detection of dopamine from the brain contributes to the implementation of fully-implantable closed-loop electronics for medical diagnosis and treatment of neurodegenerative diseases. The identification of oxidation and reduction peaks and corresponding reaction potentials from the sensor interface can be used in future systems to provide a feedback solution that stimulates the release of dopamine based on the detected redox current profile of the patient. Furthermore, long-term monitoring of neurochemical signals enables early detection of degeneration in neurotransmitter receptors and fosters development of more effective treatment for patients suffering from neurological disorders.

ACKNOWLEDGMENT

The authors would like to thank Academy of Finland (#269196) for funding this research work.

REFERENCES

[1] J. M. Beaulieu and R. R. Gainetdinov, "The physiology, signaling, and pharmacology of dopamine receptors," *Pharmacological reviews*, vol. 63, no. 1, pp. 182–217, Mar 2011.

[2] R. K. Goyal and A. Chaudhury, "Structure activity relationship of synaptic and junctional neurotransmission," *Autonomic Neuroscience*, vol. 176, no. 1-2, pp. 11–31, 2013.

[3] M. Roham, D. Covey, D. Daberkow, E. Ramsson, C. Howard, B. Heidenreich, P. Garris, and P. Mohseni, "A Wireless IC for Time-Share Chemical and Electrical Neural Recording," *IEEE Journal of Solid-State Circuits*, vol. 44, no. 12, pp. 3645–3658, Dec 2009.

[4] O. Olabode, M. Kosunen, and K. Halonen, "A current controlled oscillator based readout front-end for neurochemical sensing in 65nm cmos technology," in *2016 IEEE International Symposium on Circuits and Systems (ISCAS)*, May 2016, pp. 514–517.

[5] S. Ghoreishizadeh, S. Carrara, and G. De Micheli, "Circuit design for human metabolites biochip," in *2011 IEEE Biomedical Circuits and Systems Conference (BioCAS)*, Nov 2011, pp. 460–463.

[6] R. F. B. Turner, D. Harrison, and H. Baltes, "A CMOS potentiostat for amperometric chemical sensors," *IEEE Journal of Solid-State Circuits*, vol. 22, no. 3, pp. 473–478, 1987.

[7] E. Kaivosoja, E. Berg, A. Rautiainen, T. Palomäki, J. Koskinen, M. Paulasto-Krockel, and T. Laurila, "Improving the function of dopamine electrodes with novel carbon materials," in *2013 35th Annual International Conference of the IEEE Engineering in Medicine and Biology Society (EMBC)*, July 2013, pp. 632–634.

[8] K. H. Lee, C. D. Blaha, P. A. Garris, P. Mohseni, A. E. Horne, K. E. Bennet, F. Agnesi, J. M. Bledsoe, D. B. Lester, C. Kimble, H.-K. Min, Y.-B. Kim, and Z.-H. Cho, "Evolution of Deep Brain Stimulation: Human Electrometer and Smart Devices Supporting the Next Generation of Therapy," *Neuromodulation: Technology at the Neural Interface*, vol. 12, no. 2, pp. 85–103, 2009.

[9] T. Palomäki, E. Peltola, S. Sainio, N. Wester, O. Pitkänen, K. Kordas, J. Koskinen, and T. Laurila, "Unmodified and multi-walled carbon nanotube modified tetrahedral amorphous carbon (ta-c) films as in vivo sensor materials for sensitive and selective detection of dopamine," *Biosensors and Bioelectronics*, vol. 118, pp. 23 – 30, 2018.

[10] M. Ahmadi and G. Jullien, "Current-Mirror-Based Potentiostats for Three-Electrode Amperometric Electrochemical Sensors," *IEEE Transactions on Circuits and Systems I: Regular Papers*, vol. 56, no. 7, pp. 1339–1348, 2009.

[11] B. Nasri, T. Wu, A. Alharbi, K. You, M. Gupta, S. P. Sebastian, R. Kiani, and D. Shahrjerdi, "Hybrid cmos-graphene sensor array for subsecond dopamine detection," *IEEE Transactions on Biomedical Circuits and Systems*, vol. 11, no. 6, pp. 1192–1203, Dec 2017.

[12] B. Bozorgzadeh, D. R. Schuweiler, M. J. Bobak, P. A. Garris, and P. Mohseni, "Neurochemostat: A neural interface soc with integrated chemometrics for closed-loop regulation of brain dopamine," *IEEE Transactions on Biomedical Circuits and Systems*, vol. 10, no. 3, pp. 654–667, June 2016.

[13] B. Bozorgzadeh, D. Covey, C. Howard, P. Garris, and P. Mohseni, "A neurochemical pattern generator SoC with switched-electrode management for single-chip electrical stimulation and 9.3 μW, 78 pA

rms, 400 V/s fscv sensing," *IEEE J. Solid-State Circuits*, vol. 49, no. 4, pp. 881–895, 2014.

[14] M. H. Nazari, H. Mazhab-Jafari, L. Leng, A. Guenther, and R. Genov, "Cmos neurotransmitter microarray: 96-channel integrated potentiostat with on-die microsensors," *IEEE Transactions on Biomedical Circuits and Systems*, vol. 7, no. 3, pp. 338–348, June 2013.

[15] D. L. Robinson, A. Hermans, A. T. Seipel, and R. M. Wightman, "Monitoring rapid chemical communication in the brain," *Chemical Reviews*, vol. 108, no. 7, pp. 2554–2584, 2008.

[16] E. McAdams, A. Lackermeier, J. McLaughlin, D. Macken, and J. Jossinet, "The linear and non-linear electrical properties of the electrode-electrolyte interface," *Biosensors and Bioelectronics*, vol. 10, no. 1-2, pp. 67 – 74, 1995.

[17] Z. Guo, M.-L. Seol, M.-S. Kim, J.-H. Ahn, Y.-K. Choi, J.-H. Liu, and X.-J. Huang, "Sensitive and selective electrochemical detection of dopamine using an electrode modified with carboxylated carbonaceous spheres," *Analyst (Cambridge UK)*, vol. 138, no. 9, pp. 2683–2690, April 2013.

[18] F.-L. Chan, W.-Y. Chang, L.-M. Kuo, C.-H. Lin, S.-W. Wang, Y.-S. Yang, and M. S.-C. Lu, "An electrochemical dopamine sensor with a CMOS detection circuit," *Journal of Micromechanics and Microengineering*, vol. 18, no. 7, p. 075028, 2008.

[19] Denes Budai, Istvan Hernadi, Beatrix Meszaros, Zsolt K. Bali and Karoly Gulya, "Electrochemical responses of carbon fiber microelectrodes to dopamine in vitro and in vivo," *Acta Biologica Szegediensis*, vol. 54, no. 2, pp. 155–160, 2010.

[20] Glenn M. Walker, J.Michael Ramsey, Ralph K. Cavin; III, Daniel J.C. Herr, Celia I. Merzbacher, Victor Zhirnov, "A Framework for Bioelectronics: Discovery and Innovation," The National Institute of Standards and Technology (NIST), an agency of the U.S. Department of Commerce, Tech. Rep., Feb 2009, Semiconductor Electronics Division of NIST.

[21] T. Palomäki, S. Chumillas, S. Sainio, V. Protopopova, M. Kauppila, J. Koskinen, V. Climent, J. M. Feliu, and T. Laurila, "Electrochemical reactions of catechol, methylcatechol and dopamine at tetrahedral amorphous carbon (ta-c) thin film electrodes," *Diamond and Related Materials*, vol. 59, pp. 30 – 39, 2015.

[22] T. Laurila, S. Sainio, and M. Caro, "Hybrid carbon based nanomaterials for electrochemical detection of biomolecules," *Progress in Materials Science*, vol. 88, pp. 499–594, 2017.

[23] T. Laurila, V. Protopopova, S. Rhode, S. Sainio, T. Palomäki, M. Moram, J. M. Feliu, and J. Koskinen, "New electrochemically improved tetrahedral amorphous carbon films for biological applications," *Diamond and Related Materials*, vol. 49, pp. 62 – 71, 2014.

[24] R. L. McCreery, "Advanced carbon electrode materials for molecular electrochemistry," *Chemical Reviews*, vol. 108, no. 7, pp. 2646–2687, 2008.

[25] G. Massicotte, M. Sawan, G. De Micheli, and S. Carrara, "Multi-electrode amperometric biosensor for neurotransmitters detection," in *2013 IEEE Biomedical Circuits and Systems Conference (BioCAS)*, Oct 2013, pp. 162–165.

[26] S. Hocevar, J. Wang, R. Deo, M. Musameh, and B. Ogorevc, "Carbon Nanotube Modified Microelectrode for Enhanced Voltammetric Detection of Dopamine in the Presence of Ascorbate," *Electroanalysis*, vol. 17, no. 5-6, pp. 417–422, 2005.

[27] M.-P. Bui, C. Li, and G. Seong, "Electrochemical detection of dopamine with poly-glutamic acid patterned carbon nanotube electrodes," *BioChip Journal*, vol. 6, no. 2, pp. 149–156, 2012.

[28] A. Liu, I. Honma, and H. Zhou, "Simultaneous voltammetric detection of dopamine and uric acid at their physiological level in the presence of ascorbic acid using poly(acrylic acid)-multiwalled carbon-nanotube composite-covered glassy-carbon electrode," *Biosensors and Bioelectronics*, vol. 23, no. 1, pp. 74 – 80, 2007.

[29] S. Yang, G. Li, R. Yang, M. Xia, and L. b. c. Qu, "Simultaneous voltammetric detection of dopamine and uric acid in the presence of high concentration of ascorbic acid using multi-walled carbon nanotubes with methylene blue composite film-modified electrode," *Journal of Solid State Electrochemistry*, vol. 15, no. 9, pp. 1909–1918, 2011.

[30] Y.-R. Kim, S. Bong, Y.-J. Kang, Y. Yang, R. K. Mahajan, J. S. Kim, and H. Kim, "Electrochemical detection of dopamine in the presence of ascorbic acid using graphene modified electrodes," *Biosensors and Bioelectronics* , vol. 25, no. 10, pp. 2366 – 2369, 2010.

[31] Z.-H. Sheng, X.-Q. Zheng, J.-Y. Xu, W.-J. Bao, F.-B. Wang, and X.-H. Xia, "Electrochemical sensor based on nitrogen doped graphene: Simultaneous determination of ascorbic acid, dopamine and uric acid," *Biosensors and Bioelectronics*, vol. 34, no. 1, pp. 125 – 131, 2012.

[32] Y. Mao, Y. Bao, S. Gan, F. Li, and L. Niu, "Electrochemical sensor for dopamine based on a novel graphene-molecular imprinted polymers composite recognition element," *Biosensors and Bioelectronics*, vol. 28, no. 1, pp. 291 – 297, 2011.

[33] D. Han, T. Han, C. Shan, A. Ivaska, and L. Niu, "Simultaneous Determination of Ascorbic Acid, Dopamine and Uric Acid with Chitosan-Graphene Modified Electrode," *Electroanalysis*, vol. 22, no. 17-18, pp. 2001–2008, 2010.

[34] Y. Iwasaki and M. Morita, "Electrochemical Measurements with Interdigitated Array Microelectrodes," *Current Separations*, vol. 14, no. 1, pp. 1–8, 1995, NTT Basic Research Laboratories, Atsugi, Kanagawa 243-01, Japan.

[35] S. Martin, F. Gebara, T. Strong, and R. Brown, "A Fully Differential Potentiostat," *IEEE Sensors Journal*, vol. 9, no. 2, pp. 135–142, Feb 2009.

[36] O. Olabode, M. Kosunen, V. Unnikrishnan, T. Palomäki, T. Laurila, K. Halonen, and J. Ryynänen, "A sensor interface for neurochemical signal acquisition," in *2019 IEEE 62nd International Midwest Symposium on Circuits and Systems (MWSCAS)*, Aug 2019, pp. 390–393.

[37] X. Xing and G. G. E. Gielen, "A 42 fj/step-fom two-step vco-based delta-sigma adc in 40 nm cmos," *IEEE Journal of Solid-State Circuits*, vol. 50, no. 3, pp. 714–723, March 2015.

[38] S. Rao, K. Reddy, B. Young, and P. Hanumolu, "A deterministic digital background calibration technique for VCO-based ADCs," *IEEE J. Solid-State Circuits*, vol. 49, no. 4, pp. 950–960, 2014.

[39] V. Unnikrishnan and M. Vesterbacka, "Time-mode analog-to-digital conversion using standard cells," *IEEE Transactions on Circuits and Systems I: Regular Papers*, vol. 61, no. 12, pp. 3348–3357, Dec 2014.

[40] E. Hogenauer, "An economical class of digital filters for decimation and interpolation," *IEEE Transactions on Acoustics, Speech and Signal Processing*, vol. 29, no. 2, pp. 155–162, Apr 1981.

[41] R. Lyons, *Understanding Digital Signal Processing*, 3rd ed. Prentice Hall, Upper Saddle River, New Jersey, 2011.

[42] T. Watanabe, T. Mizuno, and Y. Makino, "An all-digital analog-to-digital converter with 12μV/LSB using moving-average filtering," *IEEE Journal of Solid-State Circuits*, vol. 38, no. 1, pp. 120–125, Jan 2003.

[43] A. Tritschler, "A Continuous Time Analog-to-Digital Converter With 90μW and 1.8μV/LSB Based on Differential Ring Oscillator Structures," in *2007. ISCAS 2007. IEEE International Symposium on Circuits and Systems*, May 2007, pp. 1229–1232.

[44] R. Muller, S. Gambini, and J. M. Rabaey, "A $0.013\text{mm}^2, 5\mu$W, DC-Coupled Neural Signal Acquisition IC With 0.5 V Supply," *IEEE Journal of Solid-State Circuits*, vol. 47, no. 1, pp. 232 –243, jan. 2012.

[45] U. Wismar, D. Wisland, and P. Andreani, "A $0.2V$ 0.44μW 20 kHz Analog to Digital $\Sigma\Delta$ Modulator with $57fJ$/conversion FoM," in *2006. ESSCIRC 2006. Proceedings of the 32nd European Solid-State Circuits Conference*, Sept 2006, pp. 187–190.

[46] Y. Li, M. Liu, C. Xiang, Q. Xie, and S. Yao, "Electrochemical quartz crystal microbalance study on growth and property of the polymer deposit at gold electrodes during oxidation of dopamine in aqueous solutions," *Thin Solid Films*, vol. 497, no. 1, pp. 270 – 278, 2006.

Olaitan Olabode was born in Lagos, Nigeria. She received B.Eng degree in Information Technology from Metropolia University of Applied Sciences, Espoo, Finland in 2011 and M.Sc degree in Micro and Nanosciences from Aalto University, Espoo, Finland in 2015, where she is currently pursuing a Ph.D. degree in Micro and Nanoelectronics at the Department. of Electronics and Nanoengineering. Her current research focuses on the design of integrated analog front-end circuits for implant applications.

Marko Kosunen (S'97−M'07) received his M.Sc, L.Sc and D.Sc (with honors) degrees from Helsinki University of Technology, Espoo, Finland, in 1998, 2001 and 2006, respectively. He is currently a Senior Researcher at Aalto University, Department of Electronics and Nanoengineering. Academic years 2017-2019 he visited Berkeley Wireless Reserarch Center, UC Berkeley, on Marie Sklodowska-Curie grant from European Union. He has authored and co-authored more than 90 journal and conference papers and holds several patents. His current research interests include programmatic circuit design methodologies, digital intensive and time-based transceiver circuits, and medical sensor electronics.

Vishnu Unnikrishnan (S'12−M'17) received the B.Tech. degree in electronics and communication engineering from Kannur University, India, in 2004, the M.Sc. degree in electrical engineering, and the Ph.D. degree in integrated circuits and systems both from Linköping University, Sweden, in 2012 and 2016 respectively. Since 2017, he is a postdoctoral researcher at the dept. of Electronics and Nanoengineering, Aalto University, Finland. From 2004 to 2009, he was with Bosch Engineering and Business Solutions. His research interests include energy-efficient integrated circuits and systems, digital-intensive radio/wire transceiver architectures, digital implementation/enhancement of analog/mixed-signal functions in integrated circuits, and time-domain signal processing.

Tommi Palomäki received his D.Sc. degree from the Department of Electrical Engineering and Automation at Aalto University in 2019. His research work focused primarily on the electrochemistry and characterization of amorphous carbon materials and the development of electrochemical sensors for the detection of neurotransmitters.

Tomi Laurila received the D.Sc. degree (with honours) from the Helsinki University of Technology in 2001. He is Associate Professor in the field of Microsystem technology at Aalto University, Finland, and holds an adjunct professorship on Electronics Reliability. He has also acted as a visiting professor in University Institute of Electrochemistry, in University of Alicante, Spain and in Neuroscience center in University of Helsinki, Finland. His groups research is focused on the computational materials science and electrochemical properties of carbon nanomaterials as well as their use in biosensing. The group is especially interested in finding connections between the atomic level and macroscopic properties through a tight combination of experiments and multilevel simulations.

Kari Halonen has received the M.Sc. degree in Electrical Engineering from the Helsinki University of Technology, Finland, in 1982, and the Ph.D. degree in Electrical Engineering from the Katholieke Universiteit Leuven, Belgium, in 1987. Since 1988 he has been with the Electronic Circuit Design Laboratory, Helsinki University of Technology (since 2011 Aalto University). From 1993 he has been an Associate Professor, and since 1997 a full professor at the Faculty of Electrical Engineering and Telecommunications. He became the Head of Electronic Circuit Design Laboratory in 1998 and he was appointed as the Head of Department of Micro- and Nanosciences, Aalto University, in 2007-2013. He specializes in CMOS and BiCMOS analog and RF integrated circuits, particularly for telecommunication and sensor applications. He is author or co-author of over 450 international and national conference and journal publications on analog and RF integrated circuits. He has been an Associate Editor of IEEE Journal of Solid-State Circuits, and an Associate Editor of IEEE Transactions on Circuits and Systems I, a Guest Editor for IEEE Journal of Solid-State Circuits, and the Technical Program Committee Chairman for European Solid-State Circuits Conference 2000 and 2011. He has been awarded the Beatrice Winner Award in ISSCC Conference 2002. He has served as a TPC member of ESSCIRC and ISSCC.

Jussi Ryynänen (S'99−M'04−SM'16) was born in Ilmajoki, Finland, in 1973. He received the M.Sc. and D.Sc. degrees in electrical engineering from the Helsinki University of Technology, Espoo, Finland, in 1998 and 2004, respectively. He is a full professor and the Head of the Department of Electronics and Nanoengineering, Aalto University, Espoo, Finland. He has authored or co-authored more than 140 refereed journal and conference papers in analog and RF circuit design. He holds seven patents on RF circuits. His research interests are integrated transceiver circuits for wireless applications. Prof. Ryynänen has served as a TPC Member for the European Solid-State Circuits Conference (ESSCIRC) and the IEEE International Solid-State Circuits Conference (ISSCC), and as a Guest Editor for the IEEE Journal of Solid-State Circuits